Formation of Sweet-Parker-Like Electron Dissipation Region in a Driven Open System

Bin LI[1)], Ritoku HORIUCHI[1,2)] and Hiroaki OHTANI[1,2)]

[1)]*The Graduate University for Advanced Studies, 322-6 Oroshi-cho, Toki 509-5292, Japan*
[2)]*National Institute for Fusion Science, 322-6 Oroshi-cho, Toki 509-5292, Japan*

(Received 23 October 2007 / Accepted 5 February 2008)

Nonlinear development of collisionless driven reconnection is investigated by making use of the electromagnetic particle simulation code "PASMO." This code is developed for an open system, which is subject to an external driving source. The electric field at the reconnection point increases, and approaches the external driving field as time goes on. After the formation of x-shaped field structure around the reconnection point, the length of the electron dissipation region continues to increase for a short time. Finally, it stops to grow and relaxes to a steady state when the ratio of the width to length is constant. Thus, Sweet-Parker-like electron dissipation region is formed in a steady state, while the reconnection rate is controlled by the driving electric field.

Keywords: driven reconnection, collisionless, Sweet-Parker-like, steady state, electrons dissipation region

DOI: 10.1585/pfr.3.S1054

1. Introduction

Magnetic reconnection occurs in a wide variety of plasma systems, e.g., collision-dominated plasmas in the solar convection zone, weakly collisional plasmas in the solar corona, collisionless plasmas in the Earth's magnetosphere, and plasmas observed in experiments such as tokamak and reversed field pinch [1, 2]. During magnetic reconnection, most magnetic energy is effectively transformed into plasma energy.

The structure of the dissipation region, where reversed magnetic field lines are dissipated and reconnected, has not been understood well for a long time. Recent experimental results [3] of a magnetic reconnection experiment (MRX) and observations from WIND satellite [4] shed new light in this research direction. Their results implied that the dissipation region has a Sweet-Parker like spatial geometry −a long and narrow current layer extends along the downstream direction.

Unfortunately, the Sweet-Parker model is simply based on classical collisional resistivity assumption, and cannot explain the time scale of fast energy release in solar flare. Therefore, it is necessary to investigate the mechanism responsible for violating the frozen-in flux constraint in the dissipation region. In a series of previous two-dimensional simulations, dissipation mechanisms are generally believed to be provided by microscale collisionless kinetic effects, i.e., the inertia effect [5, 6] and the thermal effect [7, 8] based on the non-gyrotropic meandering motion. It is implied that the evolution of collisionless reconnection is controlled by the particle kinetic effects in two dimensions.

author's e-mail: li.bin@nifs.ac.jp

In this paper, we focus on investigating the steady state of fast magnetic reconnection in a driven case based on the three-dimensional particle-in-cell (PIC) code "PASMO" [9, 10]. In our simulation around the X-line, an electron dissipation region is formed, which is extended to the downstream boundary. In a steady state, it has a rectangular shape current layer, which is a typical prediction of the Sweet-Parker model.

The outline of the paper is as follows. First we describe the simulation model, and then introduce the structure of the electron dissipation region. Finally, we discuss the simulation results.

2. Simulation Model

The simulation is performed using three-dimensional particle-in-cell (PIC) simulation code "PASMO," a two-dimensional version of which has been successfully used in previous investigations [7, 11–15].

Physical quantities at the boundary of z axis ($z = \pm z_b$) are assumed to be periodic. Upstream and downstream boundaries are set at those of y-axis ($y = \pm y_b$) and x-axis ($x = \pm x_b$), respectively.

At the upstream boundary, plasmas satisfy the frozen-in condition. By adopting an external electric field $E_z(x, t)$ at $y = \pm y_b$ along the z-axis, ions and electrons are driven into the simulation domain at the same drift velocity. The driving electric field is relatively larger within the input window size x_d around $x = 0$ during the Alfvén time $\tau_A = y_b/V_A$, where V_A is the initial average Alfvén velocity. Therefore, plasmas have greater speed within the size of the input window to make the convergent plasma flow into the center of the simulation domain, where magnetic

reconnection occurs first. The driving field approaches a uniform profile with a constant value along the upstream boundary. Magnetic fields can change spatially and temporally, according to the evolving driving electric field.

At the downstream boundary $x = \pm x_b$, plasma number density is controlled by both the charge neutrality condition and the condition of the net number flux, which is associated with the fluid velocity in the vicinity of the boundary [14]. Therefore, the plasma can freely flow in or out; the total number of particles may vary with time in this open system. The field quantities E_x, E_y and $\partial_x E_z$ are continuous at the downstream boundaries. The other components of the electromagnetic field can be obtained by solving the Maxwell equations at the boundary.

One-dimensional Harris sheet equilibrium is adopted as an initial condition, where the magnetic field and plasma pressure are given by $B_x(y) = B_0 \tanh(y/y_h)$ and $P(y) = B_0^2/8\pi \cdot \mathrm{sech}^2(y/y_h)$, respectively, with the scale height y_h. As a consequence of initially reversed magnetic field configuration, a neutral sheet appears at the center of y-axis ($y = 0$). The Lorentz force pushes plasmas toward the neutral line, whereas plasma pressure makes plasmas move away from it. Thus the initial equilibrium is maintained by two counterbalancing forces. The distribution of particles is a shifted Maxwellian with a uniform temperature $T_{i0} = T_{e0}$. We set the particle mass ratio $m_i/m_e = 100$, the ratio of plasma frequency to the electron cyclotron frequency $\omega_{pe0}/\omega_{ce0} = 2$, the strength of the inflow velocity $E_0/B_0 = -0.04$, and the ratio of input window size to inflow direction length $x_d = 1.5$ in our numerical simulations.

3. Electron Dissipation Region

In our simulation model, reconnection rate equals to the electric field at the X-line [7, 9–15]. When system relaxes to a steady state, both electric field E_z in the system and reconnection rate should be equal to the external driving electric field. After the reconnection process begins, the electric field at X-line increases, and equals to the driving field after $t\omega_{ce} = 750$. The difference between electric fields at the X-line and upstream boundary are shown in Fig. 1. However, the electric field along the downstream direction does not reach uniform profile until $t\omega_{ce} \approx 1110$, as shown in Fig. 2. Then, the electric field equates with the driving field everywhere in the system, and thus the system relaxes to the steady state.

Figure 3 shows the spatial profile of electrons current density at $t\omega_{ce} = 900$. The electron current density evolves gradually in a long and narrow rectangular region at the center of the current layer. Thus, an electron current sheet with a narrow and long shape is formed, which is the typical result predicted in the Sweet-Parker model. The current density increases from the upstream boundary to the X-line in the inflow direction, and magnetic field B_x gradient also increases. To understand the structure of the current sheet,

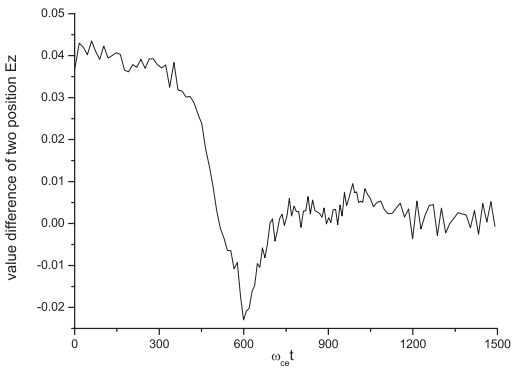

Fig. 1 Difference between values E_{z1} and E_{z2} at two positions is plotted as a function of time. E_{z1} is electric field at the X-line and E_{z2} is electric field at upstream boundaries in the steady state, during which the value of E_{z2} equals to -0.04.

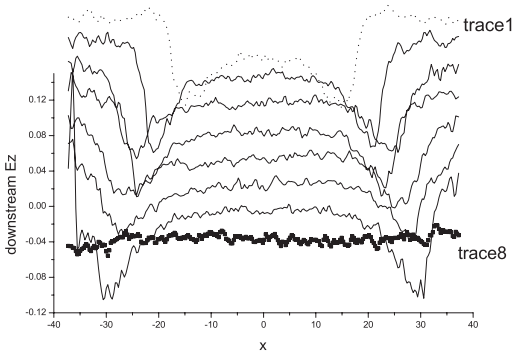

Fig. 2 Spatial profile of electric field E_z along the outflow direction at eight consecutive time periods, where trace 1 denotes the profile at $t\omega_{ce} = 662$, trace 8 at $t\omega_{ce} = 1148$. The reference level of each line is shifted vertically to avoid overlapping of lines.

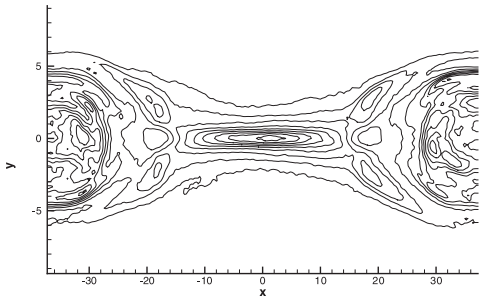

Fig. 3 Spatial profile of electrons current density at $t\omega_{ce} = 900$.

let us consider three spatial scales: electrons meandering motion scale l_{me}, skin depth $d_e = c/\omega_{pe}$, and half width of the sharp peak in the current density profile. The electron meandering scale is defined by the distance, which satisfies the condition $\rho_e(y)/y = 1$ [5, 6], where $\rho_e(y)$ is the local electron Larmor radius. The half width of the current density sharp peak is defined by the half width at 80% maximum value of the current density. In Fig. 4, time

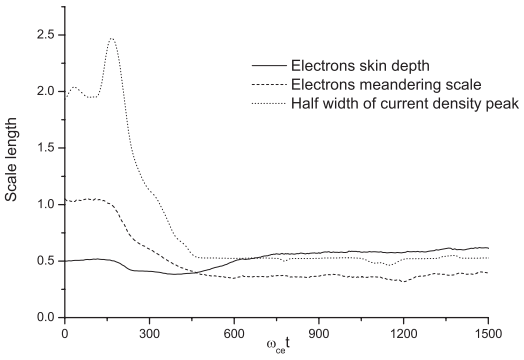

Fig. 4 Time evolution of three spatial scales; electron skin depth, electron meandering scale, and half width of current density peak.

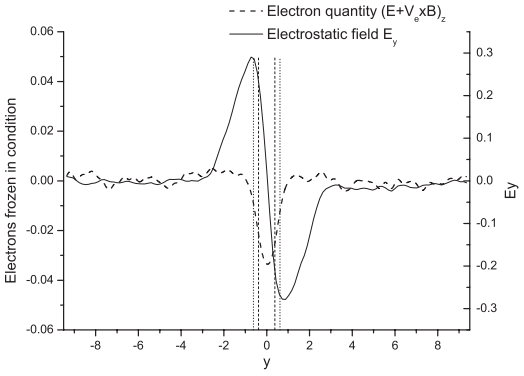

Fig. 5 Spatial profiles of the quantities $(E + v_e \times B)_z$ and electrostatic field E_y along the inflow direction at $t\omega_{ce} = 1782$. Positions of electron skin depth and meandering scale are indicated by vertical dotted lines and dashed lines, respectively.

evolution of three spatial scales defined above are plotted, where they are normalized by Debye length, and are measured along the vertical line through the X-line. The half width of the sharp peak value is close to the electrons meandering motion scale, and has similar tendency in time evolution. This result implies that electrons dynamics control the current sheet formation around the X-line, and thus a Sweet-Parker-like electrons dissipation region is generated.

In a kinetic regime non-ideal effects become significant through microscopic physical processes, and macroscopic frozen-in condition is not satisfied [8, 12–15]. Ion spatial scale, in which non-ideal effects becomes significant for ions, are larger than that for electrons. Figure 5 demonstrates the spatial profiles of $(E + v_e \times B)_z$ relating to electron frozen-in condition and the electric field E_y. Because electrons remains magnetized and ions are not magnetized in the ion dissipation region, the driving field mainly pushes the electrons inward, creating an electron-rich region inside the electron dissipation region. The in-plane electrostatic field is generated due to the charge separation in the kinetic regime, and is the largest at the edge of the electron dissipation region, as shown in Fig. 5. The violation of the electron frozen-in condition starts at electron skin depth, and becomes significant below the electron meandering scale.

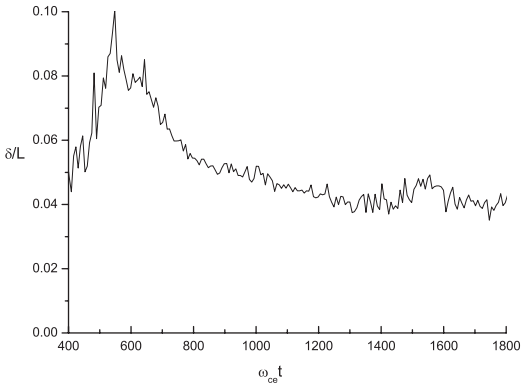

Fig. 6 Time evolution of the ratio of electron dissipation region width to its length.

In the steady state, the spatial configuration of magnetic field does not change with time, and thus the width of electron dissipation region is also expected to be a constant, which is defined by the electron skin depth. After the reconnection rate becomes a constant ($t\omega_{ce} = 750$), the skin depth also becomes a constant. Based on mass conversation of electrons, let us define the length of the electrons dissipation region using the distance from the X-line to the position where outflow speed of the electrons is maximum. The ratio of these two scales $r = d_e/l_e$ can be used to evaluate the structure of electrons dissipation region. In Fig. 6, time variation of this ratio is plotted. Although the reconnection rate, the electron skin depth and its meandering motion scale are constant (see in Figs. 1 and 4), the curve still gradually decreases. The length of electrons dissipation region increases until $t\omega_{ce} \approx 1100$, and finally the ratio becomes constant. This result corresponds to the fact that the electric field in the downstream reaches a constant profile at $t\omega_{ce} \approx 1100$ (see Fig. 2).

4. Summary

We observe that a Sweet-Parker-like electron dissipation region is formed during magnetic reconnection. Its width is determined by electron skin depth, whereas its length is defined by the distance from X-line to the position where electron outflow speed is maximum. The electron dissipation region is mainly controlled by microscopic electron dynamics.

It should be mentioned that there is a delay in the period when inflow and outflow regions relax to the steady state. The length of the electron dissipation region and downstream electric field E_z evolve after the reconnection rate at the X-line equates with the diving electric field. It is because the reconnection process has a time delay along

the inflow and outflow directions. When the reconnection takes place at the X-line, magnetic field lines reconnect there. Then, this process propagates along the outflow directions. For this reason, the closer the electric field is to the X-line in the outflow direction, the sooner it becomes stationary, as shown in Fig. 2.

The length of the electron dissipation region is determined using the position where electron outflow speed is maximum. This suggests that the electron outflow speed decreases as soon as the electrons move into the ion dissipation region, and it gradually approaches the ion outflow speed [16]. Thus, the relaxation of electron outflow speed may be determined by the cooperative action of both ion and electron dynamics.

[1] D. Biskamp, *Energy Conversion and Particle Acceleration in the Solar Corona* (Springer Berlin/Heidelberg, Germany, 2003) p.109.
[2] E. Priest and T. Forbes, *Magnetic reconnection* (Cambridge University Press, Cambridge, UK, 2000) p.322.
[3] H. Ji, M. Yamada, S. Hsu and R. Kulsrud, Phys. Rev. Lett. **80**, 3256 (1998).
[4] M. Oieroset, T.D. Phan, M. Fujimoto, R.P. Lin and R.P. Lepping, Nature. **412**, 414 (2001).
[5] M. Ottaviani and F. Porcelli, Phys. Rev. Lett. **71**, 3802 (1993).
[6] D. Biskamp, E. Schwarz and J.F. Drake, Phys. Rev. Lett. **75**, 3850 (1995).
[7] R. Horiuchi and T. Sato, Phys. Plasmas **1**, 3587 (1994).
[8] M. Hesse, K. Schindler, J. Bim and M.Kuznetsova, Phys. Plasmas **6**, 1781 (1999).
[9] H. Ohtani, R. Horiuchi and A. Ishizawa, J. Plasma Phys. **72**, 929 (2006).
[10] R. Horiuchi, H. Ohtani and A. Ishizawa, J. Plasma Phys. **72**, 953 (2006).
[11] R. Horiuchi and T. Sato, Phys. Plasmas **4**, 277 (1997).
[12] A. Ishizawa, R. Horiuchi and H. Ohtani, Phys. Plasmas **11**, 3579 (2004).
[13] W. Pei, R. Horiuchi and T. Sato, Phys. Plasmas **8**, 3251 (2001).
[14] A. Ishizawa and R. Horiuchi, Phys. Rev. Lett. **95**, 45003 (2005).
[15] W. Pei, R. Horiuchi and T. Sato, Phys. Rev. Lett. **87**, 235003 (2001).
[16] H. Karimabadi, W. Daughton and J. Scudder, Geophys. Res. Lett. **34**, 13 (2007).